ACS OMEGA

http://pubs.acs.org/journal/acsodf

Article

Carbon Black and Reduced Graphene Oxide Nanocomposite for Binder-Free Supercapacitors with Reduced Graphene Oxide Paper as the Current Collector

Mario Rapisarda, Achille Damasco, Giancarlo Abbate, and Michele Meo*

Cite This: *ACS Omega* 2020, 5, 32426−32435

Read Online

ACCESS | Metrics & More | Article Recommendations | Supporting Information

ABSTRACT: Reduced graphene oxide (rGO) is an ideal candidate for the improvement of supercapacitor (SC) performances due to its industrial-ready manufacturing process and ease of processing. In this work, rGO was used as an active binder for the manufacture of carbon black (CB) and rGO-based SCs. Being able to form a stable suspension in water, graphene oxide (GO) was initially exploited as a dispersing agent to fabricate a homogeneous slurry with CB having exclusively water as a low-cost and environment-friendly solvent. After casting on a suitable substrate, the material was subjected to thermal treatment allowing the reduction of GO to rGO, which was successively confirmed by chemical−physical analysis. An innovative current collector, consisting of high-quality rGO paper, was also proposed ensuring an improved adhesion between the active material and the substrate and a reduction of the whole weight with respect to devices fabricated using common metallic current collectors. Due to the interesting electrochemical performances, with a high specific power of 32.1 kW kg^{-1} and a corresponding specific energy of 8.8 Wh kg^{-1} at a current of 1 A g^{-1}, and the improved manufacturing process, the described "all-graphene-based" device represents a valuable candidate for the future of SCs.

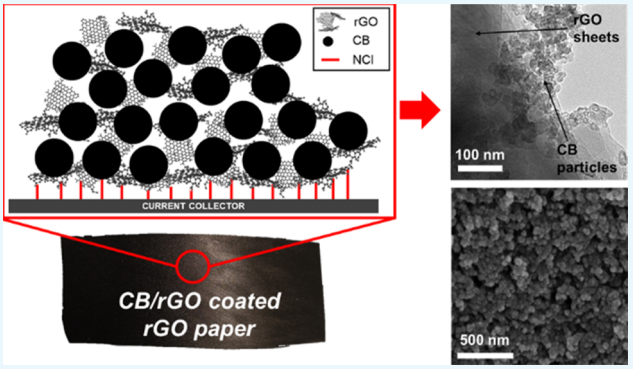

INTRODUCTION

Scientific research about SCs, being energy storage devices offering excellent performances when charge and/or discharge speeds are crucial,[1] is of huge and growing interest. Moreover, SCs can work at low temperatures and carry out many charge and discharge cycles (until 1 million). Examples of SC applications are emergency opening systems in buses and planes, UPS systems, KERS and stop-start technology in cars (especially hybrids), and the partial replacement of batteries in trucks.[1] They also operate in energy intermittence protection systems in wind or solar power generation plants,[2,3] in the energy recovery apparatus of overhead cranes and hoists, in the rail transportation industry,[4] and, recently, also in mobile devices, for powerful flashes and Wi-Fi.[5,6]

rGO is a graphene-like material produced from a reduction reaction of GO.[7,8] The latter is a functionalized graphene sheet having oxygen functional groups such as hydroxyl and carboxyl or epoxide that disrupt the conjugated network of sp^2-hybridized carbon atoms, which is the peculiarity determining the great electronic and thermal properties of pristine graphene.[9−12] Through the process of reduction, these groups can be stripped away and the hexagonal lattice of carbon atoms can be recovered. For this reason, rGO is a good electrical conductor, even if not fully comparable with pristine graphene:[13] the removal of the oxygen-containing groups causes topological defects affecting the electrical and thermal properties.[14] There are however different methods to improve the reduction process and to prevent topological defects in the wide literature about rGO.[15−20] Nowadays, one of the most common ways to obtain graphene-like materials relies on the oxidation of graphite to obtain graphite oxide (GtO).[21−23] From GtO, sheets of GO can be produced as intermediates thanks to mechanical exfoliation.[10] Besides, the direct rGO production is possible.[15,16] In numerous works, the choice of GO arises from two important advantages: it is readily soluble in water, and it can be reduced in both physical, providing energy with heat or laser,[16,17] and chemical ways.[18] However, due to the presence of oxygen functionalities, GO is an electric insulator and, therefore, the effectiveness of the reduction process becomes crucial when rGO is used in energy storage devices as SCs.

Since all kinds of commercial or experimental SCs have a high specific power, the main aim of current scientific research

Received: September 15, 2020
Accepted: November 30, 2020
Published: December 10, 2020

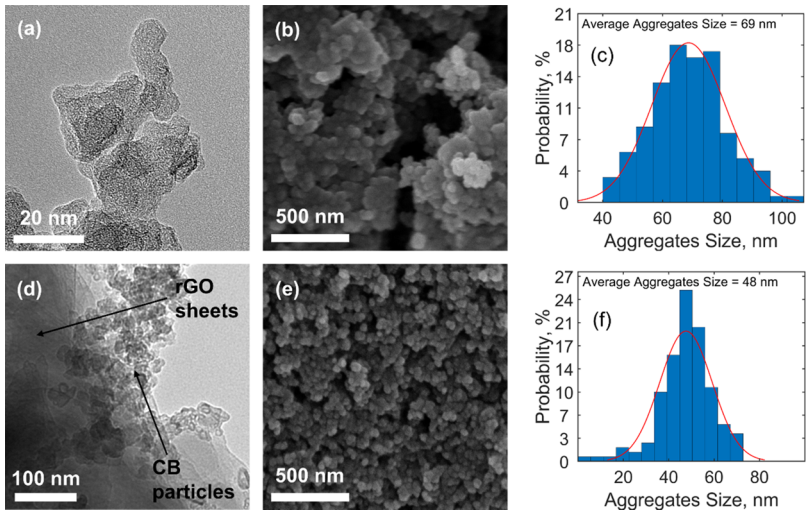

Figure 1. (a,d) TEM and (b,e) FE-SEM images of (a,b) CB_TT and (d,e) CB/GO_TT with the relative histograms of aggregate size distribution (c,f), respectively (see Table 2 in the Experimental Section for the adopted nomenclature in this work). The term referred to the current collector has been omitted since it does not affect thermal treatment results.

focuses on the improvement of the amount of stored energy, which is nowadays about 1/10 of the energy of a battery with the same mass.[24] Nonetheless, the stored energy is not the only margin of improvement: the manufacturing process and in particular its cost, scalability, and environmental impact are important to give to new SCs a concrete impingement on the technological progress. Furthermore, the final weights of the devices may be crucial for applications in the automotive and aerospace fields, as well as in portable electronics. In an SC electrode, the "active material" (i.e., the material responsible for electrical charge storage and usually consisting of porous carbons characterized by a high specific surface area like activated carbons (AC) and CB powders) needs to adhere to a current collector (i.e., the material allowing electrical current flow and usually consisting of aluminum (Al) sheets) by use of a binder. In most cases, especially in commercial SCs, the binder is a glue consisting of polymers such as polytetrafluoroethylene and polyvinylidene fluoride.[25,26] They both provide good adhesion and electrochemical stability; however, being electrically insulating polymers, they also represent a high-resistance component in the electrode. In addition, such polymers, together with the organic solvents required to obtain homogeneous slurries suitable for the coating of current collectors, are expensive and dangerous for the environment. Binders therefore represent a dead mass that is convenient to be reduced. An alternative to common binders is identified in conductive polymers such as polyaniline nanofibers, which can be used to fabricate freestanding electrodes or as a support for carbon nanotubes.[27] Their practical use is however limited by the manufacturing method: electrospinning is not readily scalable to industrial processes. In the work of Galhena et al.,[20] rGO was adopted as an alternative binder with good results. However, as in other studies,[28,29] the use of toxic and expensive organic solvents was still necessary, especially for the electrical double layer capacitors (EDLCs; i.e., a type of SC relying only on electrostatic charge storage). In hybrid SCs (HSCs; i.e., a type of SC consisting of a battery-like Faradaic electrode and an EDLC-like non-Faradaic electrode), an aqueous electrolyte was used for an rGO-based nanocomposite electrode.[30−32] For the latter, the Faradaic electrode can be made with a metal−organic or metal−sulfidic nanostructure, while the EDLC electrode can be made with carbon nanotubes evenly distributed in graphene sheets.[30−32] As the reported HSCs show promising performances, they are valuable for the future of SCs. Moreover, thanks to their hybrid nature, they can also benefit from newly developed electrodes for EDLCs based on rGO.

In this work, the fabrication of binder-free electrodes for EDLCs based on a nanocomposite of CB and rGO is proposed. A water-based slurry of CB and GO was coated to a current collector and then thermally treated through a tube furnace to promote the reduction of GO. rGO formation was confirmed by chemicophysical characterization, while its ability to behave as an "active binder" (i.e., as a material that ensures adhesion of the nanocomposite to the substrate with direct contribution to the final performance) was proven by electrochemical characterization. In addition, an innovative use of a current collector consisting of high-quality rGO paper was also tested. It derives from a high-temperature thermal treatment of GO and allows a double advantage with respect to conventional Al collectors: an improved adhesion with the nanocomposite active material under examination, thanks to the materials' affinity, and a reduced weight, thanks to a density of 1.2 g cm^{-3} against 2.7 g cm^{-3} with a comparable thickness. With the promising performances of the as-obtained samples, showing a high specific power of 32.1 kW kg^{-1} and a corresponding specific energy of 8.8 Wh kg^{-1} at a current of 1 A g^{-1}, together with the cheap, environmental-friendly, and scalable process adopted, the "all-graphene-based" device described in this study represents a valuable candidate for the future of SCs.

RESULTS AND DISCUSSION

Chemicophysical Characterization. The carbon nanocomposite behaving as the active material of the SC electrodes proposed in this research work was obtained, as described in detail in the Experimental Section, with a GO-aided homogenization of CB particles previously suspended in a mixture of water and Triton X-100 (TX100). The carbonaceous coatings obtained after drying of the slurries were physically and chemically characterized to investigate the effects of GO in the resulting nanocomposite and confirm the

https://dx.doi.org/10.1021/acsomega.0c04530
ACS Omega 2020, 5, 32426−32435

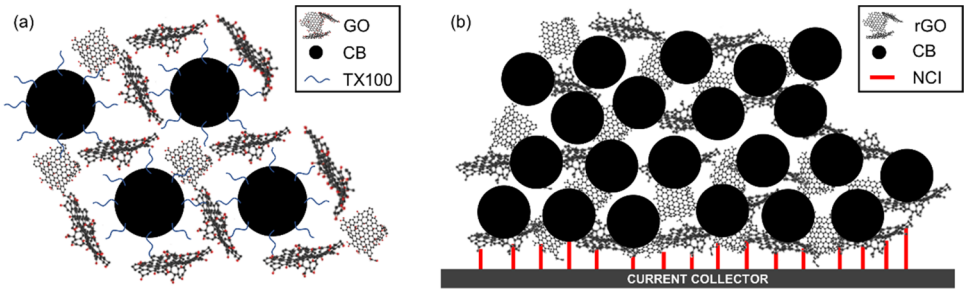

Figure 2. Proposed schemes for (a) the 3D interconnected network consisting of CB and GO with TX100 molecules as dispersers and (b) the electrically conductive carbon nanocomposite consisting of CB and rGO with noncovalent interactions (NCI) enhancing the adhesion with the current collector.

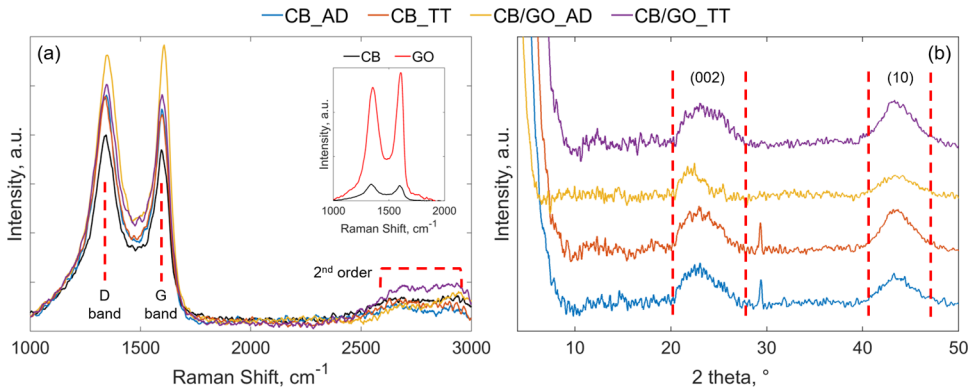

Figure 3. (a) Raman spectra of the carbonaceous coatings with untreated CB included as reference; the inset shows the comparison between the untreated CB and GO. (b) XRD patterns of the carbonaceous coatings. The term referred to the current collector has been omitted since it does not affect thermal treatment results.

reduction of GO to rGO when thermal treatment on the CB/GO slurry was applied.

CB is characterized by hierarchical morphology with particles and aggregates: particles are the fundamental building block, but they are very rarely found in isolation due to van der Waals interactions that exert a driving force for their aggregation.[33] While the initial size of pristine CB particles used for this research work ranges between 20 and 50 nm,[34] the transmission electron microscopy (TEM) images of the thermally treated carbonaceous coating obtained from the CB-only suspension in the H_2O/TX100 solution (CB_TT) show that CB particles are disrupted and reduced in size, with values ranging from 10 to 20 nm (Figure 1a). Moreover, an average agglomerate size of 69 nm was estimated from the field emission scanning electron microscopy (FE-SEM) image in Figure 1b (as depicted from the histogram with the size distribution in Figure 1c). Such a value is slightly smaller than in usual CB aggregates (which ranges between 85 and 500 nm).[33] Both phenomena suggest that the use of TX100 effectively aids the dispersion of the carbonaceous particles in water, but signs of inhomogeneity and defects in the structure of the material are still clearly visible (Figure 1b). When GO is added into the slurry, the resulting thermally treated nanocomposite (CB/GO_TT) is homogeneous and less defective (as pictured from SEM in Figure 1e). The role of TX100 is to predisperse CB in water and then to subsequently allow an intimate intercalation of GO sheets between CB particles. TX100 is a surfactant characterized by amphiphilic molecules with a hydrophilic region, consisting of polyethylene oxide chains, and a hydrophobic region, consisting of aromatic hydrocarbon chains. These are partially adsorbed by carbon, with the noncovalent $\pi-\pi$ interaction between the aromatic rings and external graphene layers on the surface of CB particles having an important function, while the hanging polyethylene oxide hydrophilic tails determine steric stabilization of CB particles against the van der Waals forces that tend instead to aggregate them.[35] In GO, thanks to the hydrophilic behavior of oxygen functional groups, water molecules can intercalate between graphene interlayer spacings, leading to stable suspensions in water.[36] When the latter is added to the predispersed CB mixture in water, the GO sheets could wrap CB particles and thus generate an interconnected 3D network (as imaged from TEM in Figure 1d and illustrated in Figure 2a) preventing CB to flocculate into bigger clusters and thus leading to smaller agglomerates (as confirmed by an estimated average size of 48 nm depicted in Figure 1f). As water evaporates in ambient conditions, the 3D structure is maintained, but it is very likely that some of its molecules would get trapped due to the strong noncovalent interactions with the CB/GO/TX100 complex. Moreover, the electrically insulating GO sheets lead to poor electrical conductivity in the electrodes, while the adsorbed TX100 molecules affect electrolyte ion diffusion. Thus, poor electrochemical performances are expected from the ambient dried samples. On the other side, when high temperatures are applied, two simultaneous phenomena lead to the formation of a highly electrically conductive carbon nanocomposite with free access to pores for electrolyte ion diffusion and enhanced adhesion thanks to noncovalent interactions with the current collector, as schematized in Figure 2b, from which remarkable electrochemical performances are likely to be developed. The first phenomenon is the thermal reduction of nonelectrically

https://dx.doi.org/10.1021/acsomega.0c04530
ACS Omega 2020, 5, 32426−32435

conductive GO to form conductive rGO, discussed in the following paragraphs with the supporting Raman spectroscopy and X-ray diffractometry (XRD) results, while the second is the complete evaporation of TX100: the latter is possible when a critical temperature of 310 °C is reached under an inert atmosphere, as demonstrated by Mitsuda et al.[37]

The Raman spectra of all the carbonaceous coatings (Figure 3a) show the existence of the G band, arising from the primary vibration mode of sp^2 atoms in rings and chains and which is a characteristic of all graphitic materials, at ~1600 cm^{-1}, and of the D band, arising from the breathing modes of sp^2 atoms induced by defects and disorder in the crystalline structure, at ~1345 cm^{-1}. These two features can be merged in their peak intensity ratio (I_D/I_G) to analyze the structure quality, where higher values of the ratio correspond to an increased disorder.[38,39] The as-calculated values for the materials under examination are reported in Table 1. Pristine CB and GO were included for reference purposes, with the higher intensity of GO peaks, explainable with a smaller crystallite size. Their I_D/I_G ratios of, respectively, 1.08 and 0.96 reveal instead their expected disordered structures. The material resulting from the ambient dried CB-only suspension in the TX100/H_2O solution shows a marginal increase in intensity of the peaks, explainable with the reduction in size of CB agglomerates during the processing in the presence of TX100. Moreover, as the I_D/I_G ratio is only slightly reduced to 1.06, the overall disorder of the crystallite structure can be assumed as unaffected. The thermally treated suspension CB_TT is almost unvaried in both peak intensity and I_D/I_G ratio (equal to 1.08), confirming that CB is inert at 550 °C under an Ar atmosphere. On the other hand, the nanocomposite obtained from the ambient dried CB/GO slurry is characterized by higher peak intensity and a I_D/I_G ratio of 0.96, proving that GO sheets in solution successfully help the disaggregation and stabilization of CB agglomerates in smaller particles, leading to a homogeneous mixture and thus confirming our previous assumption and TEM and FE-SEM results. When the thermal treatment is applied, oxygen functional groups and intercalated water are eliminated, releasing carbon dioxide (CO_2), carbon monoxide (CO), and water vapor, and thus, the conjugated network of the hexagonal lattice of carbon atoms is restored.[40] The last is the mechanism governing the electrical conductivity of graphene,[13] and the transition from the electrical insulating behavior of GO toward the conductive one of rGO is confirmed by electrochemical tests that will be described later. The generated rGO sheets show a higher degree of disorder as depicted by a I_D/I_G ratio of 1.04, a value in between those of the CB/GO nanocomposite after ambient drying (CB/GO_AD) and CB_TT, due to vacancies and topological defects on graphene layers after the release of CO_2 and CO.[40] The successful reduction of GO to rGO is furthermore proven by the increased intensity of second-order scatterings, around the graphene-associated 2D band at ~2700 cm^{-1},[41] which also shows turbostratic arrangements of graphene layers.[38]

Table 1. Raman D-to-G Band Ratios, XRD Peak Positions, Lattice Spacing, and Crystallite Sizes

sample	I_D/I_G ratio	(002) [2θ]	(10) [2θ]	d_{002} [Å]	L_C [Å]	L_A [Å]
CB_AD	1.06	23.01	43.63	3.86	18.6	40.4
CB_TT	1.08	23.09	43.63	3.85	18.1	42.1
CB/GO_AD	0.96	22.23	43.70	4.00	27.3	36.3
CB/GO_TT	1.04	23.55	43.60	3.77	17.8	41.0

The XRD patterns of the CB/GO nanocomposite and of the processed CB-only carbonaceous material used as reference, before and after thermal treatment, are presented in Figure 3b. They all show a broad peak at around 22.97°, attributable to the (002) carbon lattice and downshifted with respect to the ordered structure of graphite where the same peak is sharp and shown at 26.38°.[42] According to Bragg's law,[43] reported in eq 1, the interplanar spacing d_{002} in CB_GO_AD has a measured value of 4 Å, which is higher than the counterpart without the addition of GO (CB_AD), as observable from the values summarized in Table 1, and thus suggesting a more expanded and amorphous 3D structure of the nanocomposite (as compared to the 3.38 Å of crystalline graphite). When the thermal treatment is applied, d_{002} is almost unvaried for the CB-only carbonaceous material, while it is contracted to a value of 3.77 Å for CB_GO_TT. This is a result of the reduction of GO to rGO, which leads to the reorganization of the structure toward a more ordered fashion. Other important carbon features are the (100) and (101) lattice peaks, usually shown in graphite at 2θ values of, respectively, 42.22 and 44.39°,[42] which, for all the tested carbonaceous coatings, are merged into the broad (10) peak at around 43.64°. The latter is a consequence of turbostratic arrangements of graphene layers.[42] According to the Scherrer equation (eq 2),[44] the two main crystallite dimensions, which are the stacking height L_C and the crystallite lateral size L_A, can be estimated from, respectively, the (002) peak, using a shape factor of 0.89, and the (10) peak, with a shape factor of 1.84.[45] From their values,

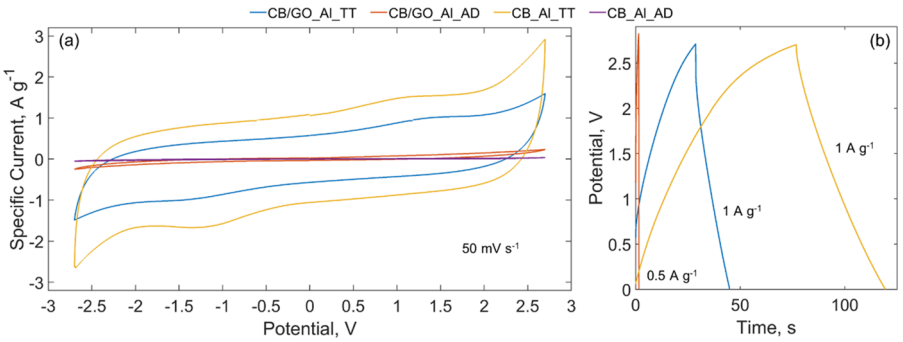

Figure 4. (a) CVs at 50 mV s^{-1} between −2.7 and +2.7 V and (b) GCs at 0.5 and 1 A g^{-1} in a 1.5 M solution of TEMA-TFB in ACN of SCs made with CB/GO_Al_TT, CB/GO_Al_AD, CB_Al_TT, and CB_Al_AD (the GC profile of the latter is omitted as the internal resistance was too high to perform measurements with comparable specific currents with respect to the other samples).

https://dx.doi.org/10.1021/acsomega.0c04530
ACS Omega 2020, 5, 32426−32435

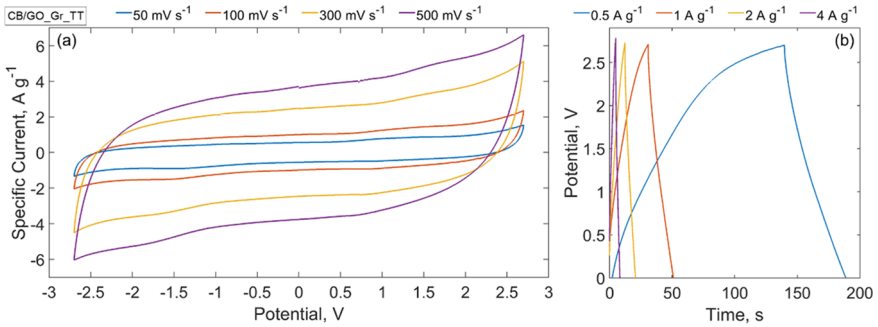

Figure 5. (a) CVs and (b) GCs of SCs made with CB/GO_Gr_TT at different scan rates, from 50 to 500 mV s^{-1}, between −2.7 and +2.7 V and different specific currents, from 0.5 to 4 A g^{-1}, in a 1.5 M solution of TEMA-TFB in ACN.

reported in Table 1, it is possible to notice the difference in both sizes between the two ambient dried samples, with and without the addition of GO. $L_C$and L_A are instead comparable after the thermal treatment. The bigger stacking height in CB/GO_AD than in CB_AD can be explained, in accordance with the interplanar spacing behavior, with an expanding effect of intercalated GO layers. In the CB-only material, almost no difference is measured in both L_C and L_A passing from the ambient dried to the thermally treated sample. In the CB/GO nanocomposite, however, a sharp decrease of L_C and a simultaneous increase of L_A are registered after the thermal treatment. These results are evidence of a hybrid structure, composed by an ordered graphitic state and an amorphous state, for the carbonaceous nanocomposite under investigation, which is typical in amorphous carbon as CB but influenced by GO intercalation. The amorphous subphase is promoted over the crystalline one in the ambient dried sample (due to a higher interplanar spacing and to a bigger crystallite size), while after the application of the thermal treatment, the reduction of GO to rGO causes an opposite effect favoring the crystalline subphase (due to the reduced spacing and the smaller crystallite size).

Electrochemical Characterization. Figure 4a,b shows the cyclic voltammetries (CVs) and galvanostatic cycles (GCs) of SCs made with the CB/GO slurry before and after thermal treatment. Also, the CVs and GCs of SCs made with the CB-only slurry before and after thermal treatment are reported for comparison. In Figure 4a, CVs are recorded using a scan rate of 50 mV s^{-1} in a potential range of −2.70 to +2.70 V; in Figure 4b, GC curves were obtained with specific currents of 0.5 A g^{-1} for CB/GO_Al_AD and of 1 A g^{-1} for CB/GO_Al_TT and CB_Al_TT. In the latter case, the different specific currents are justified as follows: using the same specific current (0.5 or 1 A g^{-1}) for all the samples, the CB/GO_Al_TT and CB_Al_TT curves would be much longer than that of CB/GO_Al_AD, leading to the impossibility of observing the trend of the latter. In Figure 4a,b, the differences between CB/GO_Al_AD and CB/GO_Al_TT prove that only with thermal treatment of GO an active material suitable for SCs can be achieved. The area under the CV curve of the thermally treated sample, CB/GO_Al_TT, is 18 times wider than that of the untreated one, CB/GO_Al_AD. In fact, the values of C_s calculated using eqs 3 and 4, reported in the Experimental Section are, respectively, 47.7 and 2.7 F g^{-1} for a scan rate of 100 mV s^{-1}. Observing Figure 4a,b, while at first glance the sample without GO in the starting slurry, CB_Al_TT, shows even better electrochemical performances, it should be noted that it actually lacks other crucial properties, such as adhesion on the current collector and mechanical stability, as shown in Figure S1 of the Supporting Information. This behavior arises from the absence of any binder, and as a consequence, such an active material can hardly be considered for the manufacture of SCs. As for GCs, for the nonthermally treated sample, the nonlinearity of the graph was too high to conduct any measurements, while it is almost linear in the discharge curve of the sample annealed at 550 °C (showing a C_s of 27.4 F g^{-1} for a specific current of 1 A g^{-1}, calculated using eqs 6 and 4). These results are a consequence of the thermal GO reduction for two reasons: since GO is an insulating material, it hinders charge transfer inside the pores (a tension drop in the discharge curve is also dominant in the CB/GO_Al_AD sample); moreover, the oxygen-containing groups of GO can lead to Faradaic reactions during the charge/discharge process, deviating from EDLC behavior and thus explaining the nonlinearities in the curve and the leakage. While the tests shown in Figure 4a,b highlight the effectiveness of the GO reduction procedure (1 h at 550 °C under Ar flow), more tests were carried out on the sample of main interest for the current work, CB/GO_Gr_TT, as described in the following paragraph and pictured in Figure 5a,b. The resulting curves of the electrochemical characterization of samples used as reference, manufactured as described in the Experimental Section, are reported in the Supporting Information (Figures S2−S4). The active mass loading, necessary to extrapolate the specific capacitance from the cell capacitance, calculated from direct measurements performed with the electrochemical workstation according to eqs 3, 4, and 6, is also reported in the Supporting Information (Table S1).

Figure 5a shows CVs between −2.70 and +2.70 V at 50, 100, 300, and 500 mV s^{-1}. The rectangular shape of these graphs proves reversibility of charge/discharge after GO reduction (i.e., electrostatic behavior only). To study the effect on specific power and adhesion in an almost "all-graphene-based SC", the trend in GCs was also analyzed. In Figure 5b, charge/discharge curves at 0.5, 1, 2, and 4 A g^{-1} are shown. Their analysis gives a specific capacitance range of 22.5−37.2 F g^{-1} and a specific energy range of 6.3−10.5 Wh kg^{-1}, while the resulting specific power range is 28.8−32.9 kW kg^{-1} (equivalent series resistance, ESR, of 30.2−26.5 Ω), calculated using, respectively, eqs 5 and 8. The specific capacitance values are lower than those in other available works in the literature because of the CB nature:[46] even though the used CB powder for the manufacture of the carbonaceous coatings under examination (BP 2000) is characterized by a high specific surface area (SSA) of 1216 m^2 g^{-1}, its micropore volume is only 0.21 cm^3 g^{-1}.[47] For the more commonly used AC, in

https://dx.doi.org/10.1021/acsomega.0c04530
ACS Omega 2020, 5, 32426−32435

which the SSA ranges from 1000 to 2000 m^2 g^{-1}, the micropore volume can reach 0.78 cm^3 g^{-1}.[48] As in a micropore (i.e., in a pore that has a less than 20 Å diameter), there are more electric charges than in a larger pore with the same area because of the ions losing the solvation sphere of the solvent; CB's SSA is less efficiently exploited than that of AC. However, it should be noted that the coupling of rGO and CB allows the optimization of other aspects of an EDLC, as shown in this research work.

The linearity of the curve from 1 A g^{-1} and above is another sign of an almost purely electrostatic behavior of this SC configuration (apart from a difference between the time of charge and discharge at 0.5 A g^{-1} due to leakage effects at low currents). In particular, at 1 A g^{-1}, a specific power of 32.1 kW kg^{-1} was obtained. Since this result is correlated with a specific energy of 8.8 Wh kg^{-1}, the SC under analysis is hence above the common limits of a commercial SC (with a maximum of 10 kW kg^{-1} of power and under 10 Wh kg^{-1} of energy).[49] The energy value derives from a combination of a specific capacitance of 31.1 F g^{-1} with a highly optimized electrolyte such as triethyl methylammonium-tetrafluoroborate (TEMA-TFB) in acetonitrile (ACN). This electrolyte uses an organic solvent with high working tension and good conductivity in addition to TEMA-TFB ions that entail cycle stability (even if this electrolyte is toxic and flammable).[50]

Figure 6 shows a comparison of SCs in the Ragone plot (i.e., a plot of the specific power versus the specific energy). It shows that, while the specific energy ranges are superimposable, when the current collector is made with rGO, there is an improvement in specific power with the same electrode. A possible explanation of this improvement could be in a different interaction of rGO in the active material when coated on a current collector consisting of the same material, such as rGO paper, rather than a metal sheet, such as Al foil: in the studied electrodes, the adhesion derives from interactions of the nonremoved oxygen-containing groups of rGO with the substrate surface.[20] While Al is a metal with an easy tendency to oxidize that often requires chemical etching to allow carbon coating, rGO paper does not need etching to form this bonding since, chemically, it is almost pure carbon. This is particularly true for the used rGO paper collector because, as in the XRD analysis on this material showed in our previous work,[51] it is characterized by a high degree of reduction of GO. Moreover, the rGO paper does not involve a discontinuity between two different materials (as for the Al−carbon interface) for the current flow during the charge/discharge process.

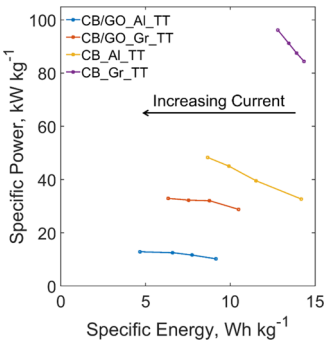

Figure 6. Ragone plot of specific power versus specific energy for SCs made with CB/GO_AL_TT, CB/GO_Gr_TT, CB_Al_TT, and CB_Gr_TT.

Surprisingly, Figure 6 shows also that the two analogous samples fabricated from the active material slurry prepared without the addition of GO perform better in both specific energy and power, in ostensible contradiction with Galhena et al.[20] It is however crucial to point out that this kind of active material has a very weak adhesion on both Al and rGO paper current collectors, which led to an extreme fragility of the as-fabricated electrodes and thus to the ease of breaking when assembling SC samples (see Figure S1 of the Supporting Information). Consequently, while these electrodes without rGO as the active binder could be adopted for the manufacture of very small devices with a delicate assembling process, they would unquestionably be not scalable. Nevertheless, the CB_Al_TT and CB_Gr_TT samples show in a clearer way that the specific power of an SC with an rGO-based current collector surpasses that of an Al-based one by a factor of almost 2 (for the maximum recorded values, the specific powers are, respectively, 98.9 and 49.4 kW kg^{-1} due to ESRs of 2.8 and 10.0 Ω). Since rGO paper mass density is less than 1/2 of Al mass density (1.2 against 2.7 g cm^{-3}), a device such as the sample CB/GO_Gr_TT could reach a 4-fold increase of the specific power when compared to a common SC, with a doubled specific energy. For the sake of clearness, this estimate omits the weight of the separator, the electrolyte, and of all the connectors of which a complete device is made.

CONCLUSIONS

In this study, a binder-free electrode was successfully manufactured using water as the only cheap and ecological solvent and GO as an alternative active binder that led to the formation of a homogeneous CB/GO nanocomposite. The material was subjected to a high-temperature (550 °C) thermal treatment to reduce GO to rGO and thus unlock its ability to actively contribute to electrical energy storage performances. The reduction effectiveness was confirmed by the increase of the I_D/I_G ratio from 0.96 to 1.04 before and after, respectively, the thermal treatment, as depicted by Raman studies and confirmed by the XRD analysis, with the reduction of the interlayer spacing d_{002} from 4.00 to 3.77 Å. The electrochemical characterization showed interesting results with a high specific power of 32.1 kW kg^{-1} and a corresponding specific energy of 8.8 Wh kg^{-1} at a specific current of 1 A g^{-1}. The latter demonstrates that the development of a cheap, environmental-friendly, and scalable manufacturing process unlocked by the complete removal of polymeric binders and organic solvents in the slurry preparation process and also the use of an innovative lightweight and high-quality current collector based on rGO for the fabrication of an "all-graphene based" device represents a valuable path for future improvements of the SC industry.

EXPERIMENTAL SECTION

Materials. CB powder (Black Pearls 2000) was supplied by Cabot Corporation. TX100 (laboratory grade), regenerated cellulose membrane filters (Whatman RC55), TEMA-TFB, and ACN were purchased from Sigma-Aldrich, while GtO powder was acquired from Xiamen TOB New Energy Technology Co. Deionized water (MilliQ), was used throughout all the experiments. All chemicals were used as received without further purification.

https://dx.doi.org/10.1021/acsomega.0c04530
ACS Omega 2020, 5, 32426−32435

Preparation of the CB/GO Slurry. CB powder (1660 mg) was added in a solution of water (13 mL) and TX100 (46.5 μL, corresponding to 50 mg) and mixed as follows: 30 min of bath ultrasonication and subsequently 2 h of magnetic stirring. The resulting CB suspension in water was then mixed with a GO dispersion of 166 mg in 20.75 mL of water (8 mg mL^{-1}) with the aid of an ultrasonicating bath. A homogeneous CB/GO (34 mg mL^{-1}) slurry was finally obtained after 12 h of further mixing using a magnetic stirrer. A CB-only slurry (34 mg mL^{-1}), without the addition of GO, was also prepared as reference.

TX100 was mixed in water with the aid of a sonicating bath in a specific amount so that its concentration with respect to CB is 3 wt %. The volume of the GO dispersion in water, previously obtained by ultrasonic exfoliation of 1200 mg of GtO in 150 mL of water, was fixed in order to achieve a mass ratio of GO/CB = 1:10.

Preparation of the rGO Paper. The rGO paper used as the current collector was prepared following the procedure described in our previous work.[51] Briefly, a GO solution in water was cast on a polyethylene terephthalate film and dried for 24 h in ambient conditions to obtain a GO film. The latter was annealed at a temperature of 1300 °C for 3 h under an argon (Ar) atmosphere and rolled to obtain a freestanding paper with a controlled thickness of 40 μm and density of 1.2 g cm^{-3}.

Fabrication of the EDLCs. The as-prepared slurries were coated on all the surface of the rGO paper serving as the current collector using the doctor blade technique. A common Al sheet was also used as the current collector for reference purposes. The coated collectors were heated at 550 °C for 1 h under an Ar atmosphere. Finally, squares of 1 cm side were cut and used as electrodes of the supercapacitor samples. Nonthermally treated electrodes, subjected instead to ambient drying for 24 h after the coating, were used as reference.

For each SC sample, two identical electrodes were laminated in the sandwich configuration using the regenerated cellulose membrane as the separator and a 1.5 M solution of TEMA-TFB in ACN as the electrolyte (0.5 mL). Heat-sealable laminating pouches and copper tape for more robust electrical connections to the current collector (the conductive tape is never in contact with the active material) were used to finish the fabrication. A total of six different samples were manufactured and tested; the adopted nomenclature and the relative features are summarized in Table 2, while a summarizing scheme of the whole manufacturing process is shown in Figure 7.

Chemicophysical Characterization. For the ease of analysis, powder samples of the coating were scratched from the current collectors of each electrode type and then treated depending on the characterization technique. TEM (JEOL JEM-2100Plus) and FE-SEM (JEOL JSM-6301F FESEM) were used to characterize the structures and morphologies of particles and agglomerates constituting the carbonaceous nanocomposite. The powdered samples were subsequently sonicated and drop-cast on TEM grids for TEM analysis, while they were deposited on conductive carbon adhesive tabs for FE-SEM analysis. The obtained images from TEM and FE-SEM were then processed with the software ImageJ to extrapolate the features of interest.

Chemical properties were investigated through Raman spectroscopy (inVia Raman microscope from Renishaw) using a 523 nm laser source (IK Series He-Cd).The crystalline structures of the blends were analyzed with transmission powder XRD (STOE STADI P) using a Cu Kα generator with 1.54 Å of wavelength. The powdered samples were deposited on regular microscope slides for Raman spectral collection, while they were mounted on specific sample holders for XRD measurements. XRD data were processed to obtain the interplanar spacing d in crystal lattices, following Bragg's law (eq 1),[43] and to estimate crystallite size L, using the Scherrer equation (eq 2)[44]

$$d = \frac{\lambda}{2 \sin \theta} \tag{1}$$

$$L = \frac{K\lambda}{B \cos \varphi} \tag{2}$$

where λ is the radiation wavelength, θ is the scattering angle of the corresponding lattice, K is a shape factor, B is the line broadening at half-maximum intensity of the peak, and φ is the corresponding scattering angle.

Table 2. Summary of Fabricated and Tested Supercapacitor Samples with the Adopted Nomenclature

sample[a]	slurry composition	current collector	thermal treatment
CB_Al_AD	CB-only in TX100/H_2O	Al	No
CB_Al_TT	CB-only in TX100/H_2O	Al	Yes
CB_Gr_TT	CB-only in TX100/H_2O	rGO paper	Yes
CB/GO_Al_AD	CB/GO in TX100/H_2O	Al	No
CB/GO_Al_TT	CB/GO in TX100/H_2O	Al	Yes
CB/GO_Gr_TT	CB/GO in TX100/H_2O	rGO paper	Yes

[a]AD is the abbreviation of ambient drying, TT is the abbreviation of thermally treated, and Gr is used to refer to the rGO paper used as the current collector.

Electrochemical Characterization. The electrochemical performances of SC samples fabricated as previously described were evaluated using a μAUTOLAB-BIII-FRA2 electrochemical workstation from Metrohm in a two-electrode configuration (Figure 7). Two different techniques were exploited, all using the aforementioned workstation: CV and GCs.

CV curves were analyzed, and the following formula was applied to calculate cell capacitances C

$$C = \frac{1}{2\nu\Delta E} \oint I(E)\mathrm{d}E = [\mathrm{F}] \tag{3}$$

where ν is the scan rate, ranging from 50 to 500 mV s^{-1} in current tests, E is the potential expressed in volts (V) with ΔE as the potential excursion, between −2.7 and 2.7 V (to better verify the EDLC behaviors of the samples, as previously discussed), and the integral represents the area inside the curve, which corresponds to the charge accumulated in the SC (with a factor of 0.5 that normalizes the repeated area of the CV curve due to opposite sign scans). The specific capacitance C_s was obtained as follows

$$C_s = 4 \times \frac{C}{m} = [\mathrm{F\ g^{-1}}] \tag{4}$$

https://dx.doi.org/10.1021/acsomega.0c04530
ACS Omega 2020, 5, 32426−32435

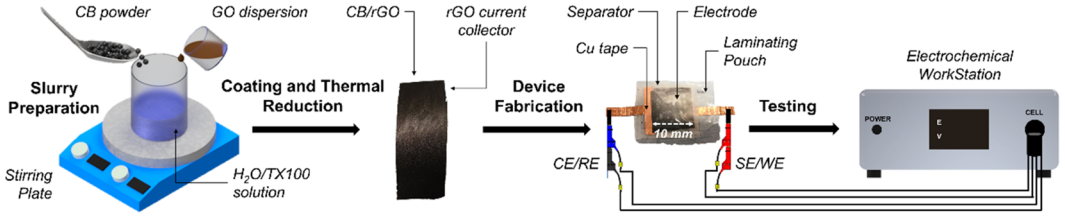

Figure 7. Scheme of the manufacturing process showing also the electrochemical workstation. CB/rGO indicates the carbonaceous nanocomposite used as the active material. CE, RE, SE, and WE indicate, respectively, the counter electrode, reference electrode, sensing electrode, and working electrode. Images by the author M. Rapisarda.

where C is the capacitance of the cell measured in the electrochemical tests while m is the mass of both electrodes expressed in grams (g). The multiplier of 4 adjusts the capacitance of the cell and the combined mass of two electrodes to the capacitance and mass of a single electrode because each electrode has a mass of $m/2$ and an EDLC is equivalent to two SCs in series with half the capacitance of a single electrode. Moreover, the specific energy U_s was determined with the following

$$U_s = \frac{1}{2 \times 3.6 \times m} \mathrm{CE}_{\max}{}^2 = [\mathrm{Wh\ kg^{-1}}] \quad (5)$$

where E_{max} is the maximum applied potential and 3.6 is a factor used for the conversion of the energy from joule to watt-hour (Wh) and of the mass from grams to kilograms (kg).

GC curves were obtained using specific currents of 0.5, 1, 2, and 4 A g^{-1}, in the potential range of 0−2.70 V. The capacitance was also calculated through the discharging part of the GC curves by the formula

$$C = \frac{I\Delta t}{\Delta E} = [\mathrm{F}] \quad (6)$$

where I is the constant discharging current, expressed in ampere, and Δt is the time interval, in seconds, of the discharge potential range ΔE. The specific capacitance and the specific energy were determined as in the previous case. Furthermore, the ESR can be estimated through the initial tension drop δE of the GC according to the following formula

$$\mathrm{ESR} = \frac{\delta E}{2I} = [\Omega] \quad (7)$$

The specific power P_S of SCs depends on the ESR and the maximum reached tension during the test as expressed in the following equation

$$P_S = \frac{E_{\max}{}^2}{4 \times \mathrm{ESR} \times m} = [\mathrm{kW\ kg^{-1}}] \quad (8)$$

The specific capacitance and the specific energy from the two tests just described usually show comparable results. However, thanks to the extra information obtainable from GCs, a Ragone plot can also be drawn to picture the tradeoff between the energy and power of electrical energy storage devices.

■ ASSOCIATED CONTENT

Supporting Information

The Supporting Information is available free of charge at https://pubs.acs.org/doi/10.1021/acsomega.0c04530.

Qualitative comparison of the adhesion of the active material on the current collector and of its mechanical integrity between CB/GO_Gr_TT and CB_Gr_TT; additional figures for CVs and GCs of CB/GO_Al_TT, CB_Al_TT, and CB_Gr_TT; comparison of the four devices of Figure 6 in terms of active mass loading, capacitance, and specific capacitance (PDF)

■ AUTHOR INFORMATION

Corresponding Author

Michele Meo − *Department of Mechanical Engineering, University of Bath, Bath BA2 7AY, U.K.*; Email: m.meo@bath.ac.uk

Authors

Mario Rapisarda − *Department of Mechanical Engineering, University of Bath, Bath BA2 7AY, U.K.*

Achille Damasco − *Dipartimento di Scienze Fisiche "Ettore Pancini", Università degli Studi di Napoli "Federico II", 80126 Naples, Italy*

Giancarlo Abbate − *Dipartimento di Scienze Fisiche "Ettore Pancini", Università degli Studi di Napoli "Federico II", 80126 Naples, Italy*

Complete contact information is available at: https://pubs.acs.org/10.1021/acsomega.0c04530

Author Contributions

M.M. and G.A. designed the project. M.R. and A.D. performed the experiments. M.R. wrote the paper with support from A.D. All authors contributed to the general discussion. All authors have read and agreed to the published version of the manuscript.

Notes

The authors declare no competing financial interest.

■ ACKNOWLEDGMENTS

We acknowledge Prof. Frank Marken, Dr. Elena Madrid, and Budi Riza Putra Putra of the Department of Chemistry of the University of Bath for their hospitality and advice. We acknowledge also in the same university Dr. Salman Shahid of the Department of Chemical Engineering for sharing his experiences about carbon and surfactants. Finally, we acknowledge the Material and Chemical Characterisation Facility (MC^2) at the University of Bath (https://doi.org/10.15125/mx6j-3r54) for technical support and assistance in this work.

■ REFERENCES

(1) Abbate, G. S. E.; Damasco, A. Supercapacitor for Future Energy Storage. In *Sustaining Resources for Tomorrow. Green Energy and Technology*; Stagner, J. A., Ting, D. S.-K. *(eds)*, Springer: Cham 2020.

(2) Abbey, C.; Joos, G. Supercapacitor Energy Storage for Wind Energy Applications. *IEEE Trans. Ind. Appl.* **2007**, *43*, 769−776.

(3) Hassanalieragh, M.; Soyata, T.; Nadeau, A.; Sharma, G. UR-SolarCap: An Open Source Intelligent Auto-Wakeup Solar Energy

Harvesting System for Supercapacitor-Based Energy Buffering. *IEEE Access* **2016**, *4*, 542−557.
(4) Ghaviha, N.; Campillo, J.; Bohlin, M.; Dahlquist, E. Review of Application of Energy Storage Devices in Railway Transportation. *Energy Procedia* **2017**, *105*, 4561−4568.
(5) Song, Z.; Hou, J.; Hofmann, H.; Li, J.; Ouyang, M. Sliding-mode and Lyapunov function-based control for battery/supercapacitor hybrid energy storage system used in electric vehicles. *Energy* **2017**, *122*, 601−612.
(6) Carignano, M. G.; Costa-Castelló, R.; Roda, V.; Nigro, N. M.; Junco, S.; Feroldi, D. Energy management strategy for fuel cell-supercapacitor hybrid vehicles based on prediction of energy demand. *J. Power Sources* **2017**, *360*, 419−433.
(7) Stobinski, L.; Lesiak, B.; Malolepszy, A.; Mazurkiewicz, M.; Mierzwa, B.; Zemek, J.; Jiricek, P.; Bieloshapka, I. Graphene oxide and reduced graphene oxide studied by the XRD, TEM and electron spectroscopy methods. *J. Electron Spectrosc. Relat. Phenom.* **2014**, 145−154.
(8) Compton, O. C.; Nguyen, S. T. Graphene oxide, highly reduced graphene oxide, and graphene: versatile building blocks for carbon-based materials. *Small* **2010**, *6*, 711−723.
(9) Lerf, A.; He, H.; Forster, M.; Klinowski, J. Structure of Graphite Oxide Revisited. *J. Phys. Chem. B* **1998**, *102*, 4477−4482.
(10) Dreyer, D. R.; Park, S.; Bielawski, C. W.; Ruoff, R. S. The chemistry of graphene oxide. *Chem. Soc. Rev.* **2010**, *39*, 228−240.
(11) Novoselov, K. S.; Geim, A. K.; Morozov, S. V.; Jiang, D.; Zhang, Y.; Dubonos, S. V.; Grigorieva, I. V.; Firsov, A. A. Electric Field Effect in Atomically Thin Carbon Films. *Science* **2004**, *306*, 666−669.
(12) Balandin, A. A. Thermal properties of graphene and nanostructured carbon materials. *Nat. Mater.* **2011**, *10*, 569−581.
(13) Pei, S.; Cheng, H.-M. The reduction of graphene oxide. *Carbon* **2012**, *50*, 3210−3228.
(14) Bagri, A.; Mattevi, C.; Acik, M.; Chabal, Y. J.; Chhowalla, M.; Shenoy, V. B. Structural evolution during the reduction of chemically derived graphene oxide. *Nat. Chem.* **2010**, *2*, 581−587.
(15) El-Kady, M. F.; Kaner, R. B. Scalable fabrication of high-power graphene micro-supercapacitors for flexible and on-chip energy storage. *Nat. Commun.* **2013**, *4*, 1475.
(16) Yang, H.; Kannappan, S.; Pandian, A. S.; Jang, J.-H.; Lee, Y. S.; Lu, W. Nanoporous graphene materials by low-temperature vacuum-assisted thermal process for electrochemical energy storage. *J. Power Sources* **2015**, *284*, 146−153.
(17) Jeong, H.-K.; Lee, Y. P.; Jin, M. H.; Kim, E. S.; Bae, J. J.; Lee, Y. H. Thermal stability of graphite oxide. *Chem. Phys. Lett.* **2009**, *470*, 255−258.
(18) De Silva, K. K. H.; Huang, H.-H.; Joshi, R. K.; Yoshimura, M. Chemical reduction of graphene oxide using green reductants. *Carbon* **2017**, *119*, 190−199.
(19) Zhu, Y.; Stoller, M. D.; Cai, W.; Velamakanni, A.; Piner, R. D.; Chen, D.; Ruoff, R. S. Exfoliation of Graphite Oxide in Propylene Carbonate and Thermal Reduction of the Resulting Graphene Oxide Platelets. *ACS Nano* **2010**, *4*, 1227−1233.
(20) Galhena, D. T. L.; Bayer, B. C.; Meyer, J. C.; Hofmann, S.; Amaratunga, G. A. J. Reduced Graphene Oxide as a Monolithic Multifunctional Conductive Binder for Activated Carbon Super-capacitors. *ACS Omega* **2018**, *3*, 9246−9255.
(21) Brodie, B. C. XIII. On the atomic weight of graphite. *Philos. Trans. R. Soc. London* **1859**, *149*, 249−259.
(22) Hummers, W. S., Jr.; Offeman, R. E. Preparation of Graphitic Oxide. *J. Am. Chem. Soc.* **1958**, *80*, 1339−1339.
(23) Chen, J.; Yao, B.; Li, C.; Shi, G. An improved Hummers method for eco-friendly synthesis of graphene oxide. *Carbon* **2013**, *64*, 225−229.
(24) Rolison, D. R.; Nazar, L. F. Electrochemical energy storage to power the 21st century. *MRS Bull.* **2011**, *36*, 486−493.
(25) Abbas, Q.; Pajak, D.; Frąckowiak, E.; Béguin, F. Effect of binder on the performance of carbon/carbon symmetric capacitors in salt aqueous electrolyte. *Electrochim. Acta* **2014**, *140*, 132−138.
(26) Chmiola, J.; Largeot, C.; Taberna, P.-L.; Simon, P.; Gogotsi, Y. Desolvation of Ions in Subnanometer Pores and Its Effect on Capacitance and Double-Layer Theory. *Angew. Chem., Int. Ed.* **2008**, *47*, 3392−3395.
(27) Simotwo, S. K.; DelRe, C.; Kalra, V. Supercapacitor Electrodes Based on High-Purity Electrospun Polyaniline and Polyaniline−Carbon Nanotube Nanofibers. *ACS Appl. Mater. Interfaces* **2016**, *8*, 21261−21269.
(28) Xu, B.; Wang, H.; Zhu, Q.; Sun, N.; Anasori, B.; Hu, L.; Wang, F.; Guan, Y.; Gogotsi, Y. Reduced graphene oxide as a multi-functional conductive binder for supercapacitor electrodes. *Energy Storage Mater.* **2018**, *12*, 128−136.
(29) Choi, J.-H.; Lee, C.; Cho, S.; Moon, G. D.; kim, B.-s.; Chang, H.; Jang, H. D. High capacitance and energy density supercapacitor based on biomass-derived activated carbons with reduced graphene oxide binder. *Carbon* **2018**, *132*, 16−24.
(30) Xu, S.; Liu, R.; Shi, X.; Ma, Y.; Hong, M.; Chen, X.; Wang, T.; Li, F.; Hu, N.; Yang, Z. A dual CoNi MOF nanosheet/nanotube assembled on carbon cloth for high performance hybrid super-capacitors. *Electrochim. Acta* **2020**, *342*, 136124.
(31) Xu, S.; Su, C.; Wang, T.; Ma, Y.; Hu, J.; Hu, J.; Hu, N.; Su, Y.; Zhang, Y.; Yang, Z. One-step electrodeposition of nickel cobalt sulfide nanosheets on Ni nanowire film for hybrid supercapacitor. *Electro-chim. Acta* **2018**, *259*, 617−625.
(32) Xu, S.; Wang, T.; Ma, Y.; Jiang, W.; Wang, S.; Hong, M.; Hu, N.; Su, Y.; Zhang, Y.; Yang, Z. Cobalt Doping To Boost the Electrochemical Properties of Ni@Ni_3S_2 Nanowire Films for High-Performance Supercapacitors. *ChemSusChem* **2017**, *10*, 4056−4065.
(33) I. C. B. A. *Carbon Black User's Guide: Safety, Health & Environmental Information*; International carbon black association: 2016.
(34) Weingarth, D.; Drumm, R.; Foelske-Schmitz, A.; Kötz, R.; Presser, V. An electrochemical *in situ* study of freezing and thawing of ionic liquids in carbon nanopores. *Phys. Chem. Chem. Phys.* **2014**, *16*, 21219−21224.
(35) González-García, C. M.; González-Martín, M. L.; Gómez-Serrano, V.; Bruque, J. M.; Labajos-Broncano, L. Determination of the Free Energy of Adsorption on Carbon Blacks of a Nonionic Surfactant from Aqueous Solutions. *Langmuir* **2000**, *16*, 3950−3956.
(36) Paredes, J. I.; Villar-Rodil, S.; Martínez-Alonso, A.; Tascón, J. M. D. Graphene Oxide Dispersions in Organic Solvents. *Langmuir* **2008**, *24*, 10560−10564.
(37) Mitsuda, K.; Kimura, H.; Murahashi, T. Evaporation and decomposition of Triton X-100 under various gases and temperatures. *J. Mater. Sci.* **1989**, *24*, 413−419.
(38) Pimenta, M. A.; Dresselhaus, G.; Dresselhaus, M. S.; Cançado, L. G.; Jorio, A.; Saito, R. Studying disorder in graphite-based systems by Raman spectroscopy. *Phys. Chem. Chem. Phys.* **2007**, *9*, 1276−1290.
(39) Ferrari, A. C. Raman spectroscopy of graphene and graphite: Disorder, electron−phonon coupling, doping and nonadiabatic effects. *Solid State Commun.* **2007**, *143*, 47−57.
(40) Schniepp, H. C.; Li, J.-L.; McAllister, M. J.; Sai, H.; Herrera-Alonso, M.; Adamson, D. H.; Prud'homme, R. K.; Car, R.; Saville, D. A.; Aksay, I. A. Functionalized Single Graphene Sheets Derived from Splitting Graphite Oxide. *J. Phys. Chem. B* **2006**, *110*, 8535−8539.
(41) Ferrari, A. C.; Meyer, J. C.; Scardaci, V.; Casiraghi, C.; Lazzeri, M.; Mauri, F.; Piscanec, S.; Jiang, D.; Novoselov, K. S.; Roth, S.; Geim, A. K. Raman Spectrum of Graphene and Graphene Layers. *Phys. Rev. Lett.* **2006**, *97*, 187401.
(42) Krishnankutty, N.; Vannice, M. A. Effect of Pretreatment on Surface Area, Porosity, and Adsorption Properties of a Carbon Black. *Chem. Mater.* **1995**, *7*, 754−763.
(43) Bragg, W. H.; Bragg, W. L. The reflection of X-rays by crystals. *Proc. R Soc. London* **1913**, *88*, 246−248.
(44) Scherrer, P. Bestimmung der Größe und der inneren Struktur von Kolloidteilchen mittels Röntgenstrahlen. In *Kolloidchemie Ein Lehrbuch*; 1912, Springer: Berlin, 387−409.

https://dx.doi.org/10.1021/acsomega.0c04530
ACS Omega 2020, 5, 32426−32435

(45) Biscoe, J.; Warren, B. E. An X-Ray Study of Carbon Black. *J. Appl. Phys.* **1942**, *13*, 364−371.
(46) Naoi, K.; Simon, P. New Materials and New Configurations for Advanced Electrochemical Capacitors. *J. Electrochem. Soc.* **2008**, *17*, 34−37.
(47) Mydul Islam, A. K. M.; Hwang, J.-I.; Lee, S.-E.; Kim, J.-E. Comparative study of carbon black and activated carbon adsorbents for removal of carbofuran from aqueous solution. *Desalin. Water Treat.* **2016**, *57*, 21512−21523.
(48) Shiraishi, S. Highly-Durable Carbon Electrode for Electrochemical Capacitors. *Boletin del Grupo Español del Carbón* **2013**, *28*, 18−24.
(49) Simon, P.; Gogotsi, Y. Materials for electrochemical capacitors. *Nat. Mater.* **2008**, *7*, 845−854.
(50) Xia, L.; Yu, L.; Hu, D.; Chen, G. Z. Electrolytes for electrochemical energy storage. *Mater. Chem. Front.* **2017**, *1*, 584−618.
(51) Rapisarda, M.; Meo, M. *Multifunctional reduced graphene oxide coating on laminated composites. Mater. Today: Proc.* 2020, DOI: 10.1016/j.matpr.2020.01.612.

https://dx.doi.org/10.1021/acsomega.0c04530
ACS Omega 2020, 5, 32426−32435